

## Supporting Information

### High Pseudocapacitance Boosts Monolithic Porous Carbon Cloth/Closely Packed TiO<sub>2</sub> Nanodots as Anode of All-Flexible Sodium Ion Battery

Bei Long,<sup>a</sup> Jingnan Zhang,<sup>a</sup> Lei Luo,<sup>b</sup> Gangfeng Ouyang,<sup>b</sup> Muhammad-Sadeeq Balogun,<sup>c</sup> Shuqin Song\*<sup>a</sup> and Yexiang Tong\*<sup>ab</sup>

*a* The Key Lab of Low-Carbon Chemistry & Energy Conservation of Guangdong Province, School of Materials Science and Engineering, Sun Yat-sen University, Guangzhou 510275 P. R. China

*b* MOE of the Key Laboratory of Bioinorganic and Synthetic Chemistry, KLGHEI of Environment and Energy Chemistry, School of Chemistry, Sun Yat-sen University, Guangzhou 510275 P. R. China

*c* College of Materials Science and Engineering, Hunan University, Changsha 410012 P. R. China

#### The calculation of capacitive contribution

The capacitive and diffusion-controlled capacity can be calculated by the following equation:<sup>1-4</sup>

$$I(V) = k_1v + k_2v^{1/2} \quad (1)$$

where  $k_1$  and  $k_2$  are the capacitive and the diffusion-controlled constants for the total

capacity at a particular voltage respectively, while  $\nu$  is the sweep rate. To obtain  $k_1$  and  $k_2$ , the CV curves at different scan rate (0.2, 0.4, 0.6, 0.8, 1, 3, 5 and 8  $\text{mV s}^{-1}$ ) are collected. During the potential range from 0.13 to 3.0 V, the current values of eight CV curves at the interval of every 0.05 V (such as 3.00, 2.95 and 2.90 V) are recorded. A set of current values (eight) at a particular potential and scan rates ( $\nu$ ) are substituted in equation (1). We can get the values of  $k_1$  and  $k_2$  and capacitive capacity ( $k_1\nu$ ) at this potential. At same scan rate, the ratio of the area consisting of all  $k_1\nu$  at the interval of every 0.05 V and CV curves area is the percentage of capacitive contribution.

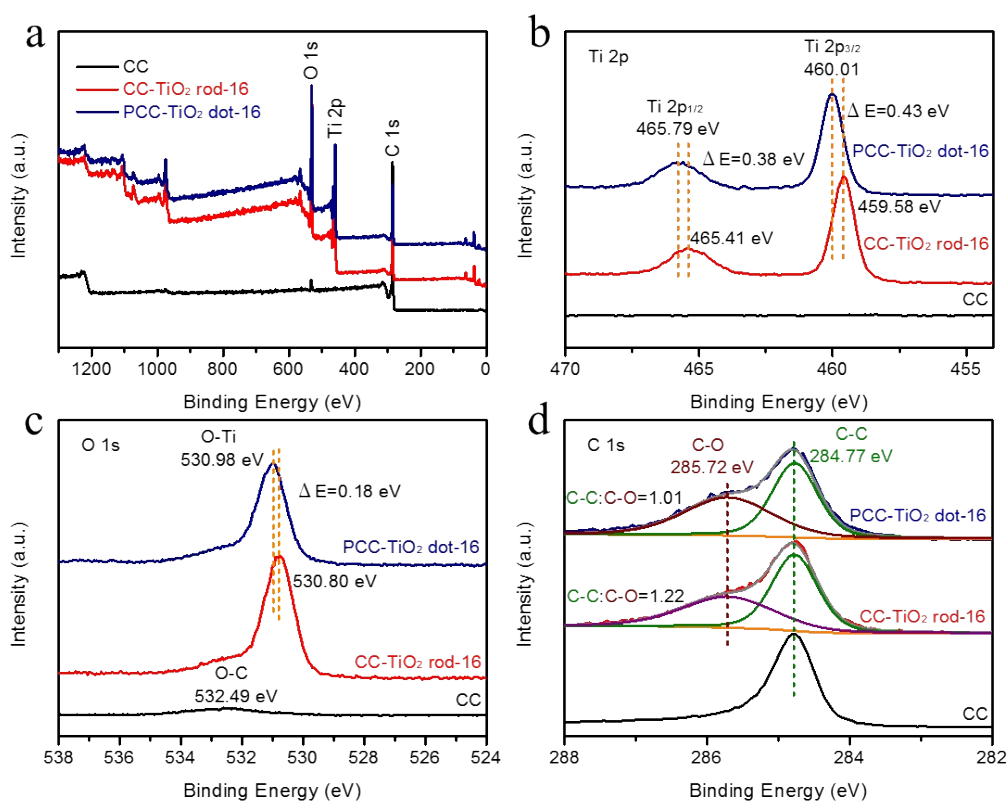


**Figure S1.** (a) XPS survey, (b) Ti 2p, (c) O 1s and (d) C 1s spectra of CC and CC-TiO<sub>2</sub> rod-16 and PCC-TiO<sub>2</sub> dot-16.

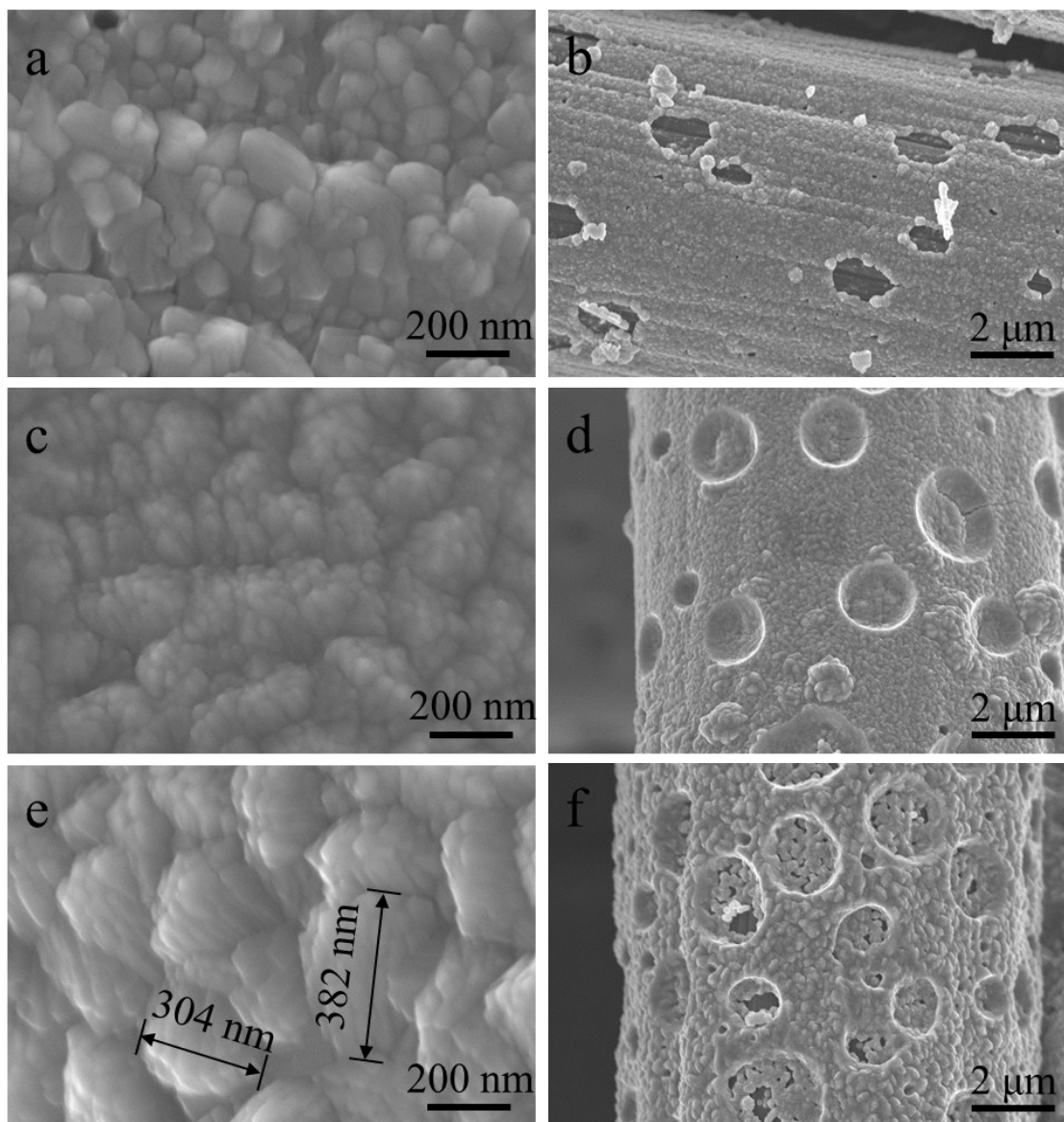


**Figure S2.** SEM images of (a,b) PCC-TiO<sub>2</sub> dot-8, (c,d) PCC-TiO<sub>2</sub> dot-12 and (e,f) PCC-TiO<sub>2</sub> dot-20.

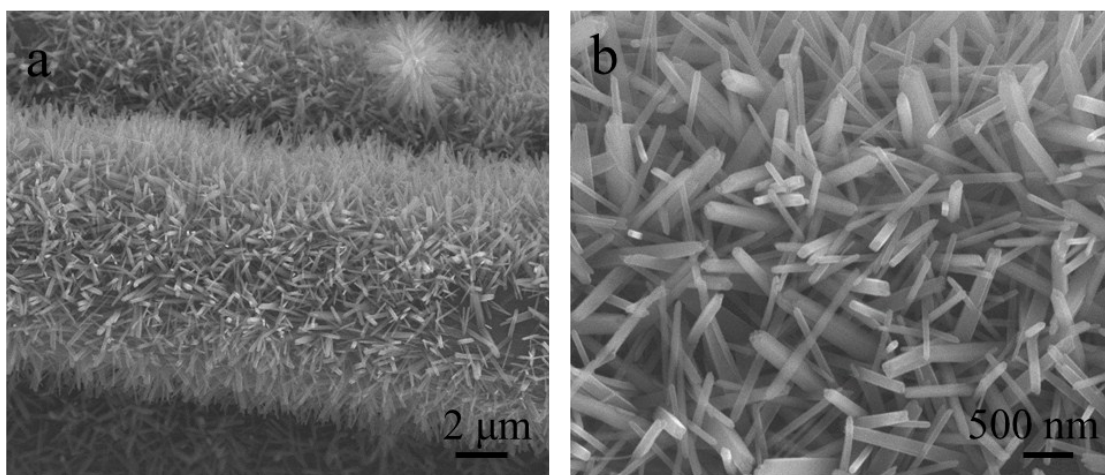


**Figure S3.** SEM images of CC-TiO<sub>2</sub> rod-16.

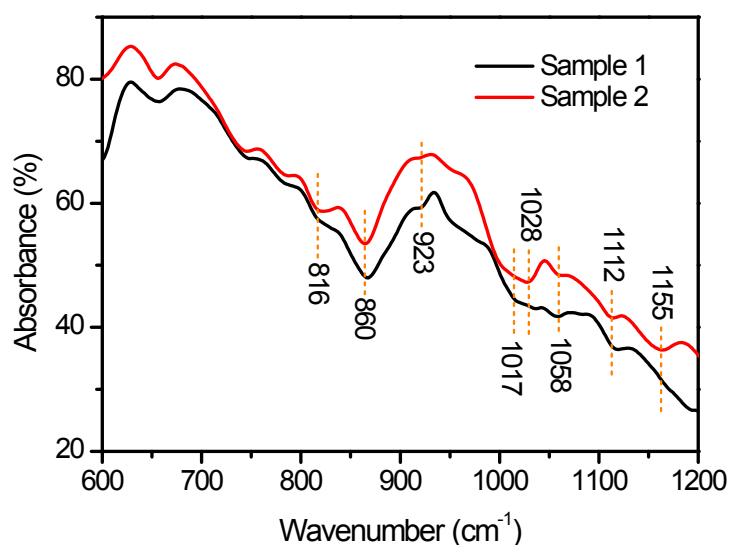


**Figure S4.** FTIR spectra of polybutylene.

Polybutylene can be obtained by collecting the solid after hydrothermal reaction. In FTIR spectra (Fig. S4), the characteristic peaks at 816, 860, 923, 1017, 1028, 1058, 1112 and 1155 cm<sup>-1</sup> are assigned to polybutylene.<sup>5-8</sup> The peak at 923 cm<sup>-1</sup> is ascribed to the CH<sub>2</sub> and CH<sub>3</sub> rocking vibrations of polybutylene.<sup>5-8</sup> The peak at 1155 cm<sup>-1</sup> corresponds to the backbone CH<sub>2</sub> bending vibrations and C-C covalent-bond vibrations of polybutylene.<sup>5-8</sup> While the undefined peaks reflect the generation of side product.

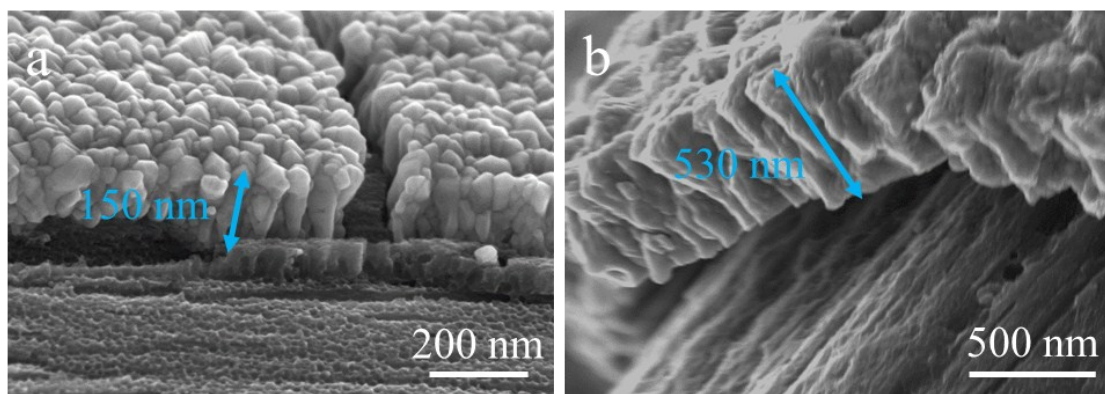


**Figure S5.** Cross section SEM images of (a) PCC-TiO<sub>2</sub> dot-4 and (b) PCC-TiO<sub>2</sub> dot-16.

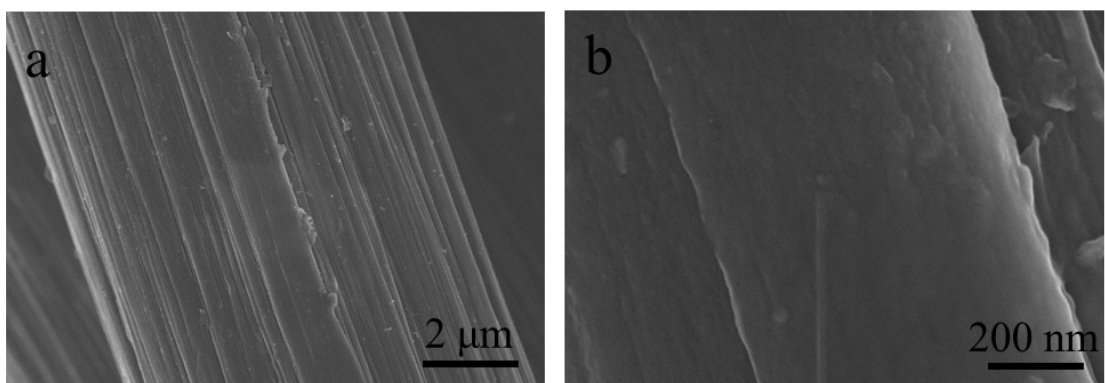


**Figure S6.** SEM images of CC.

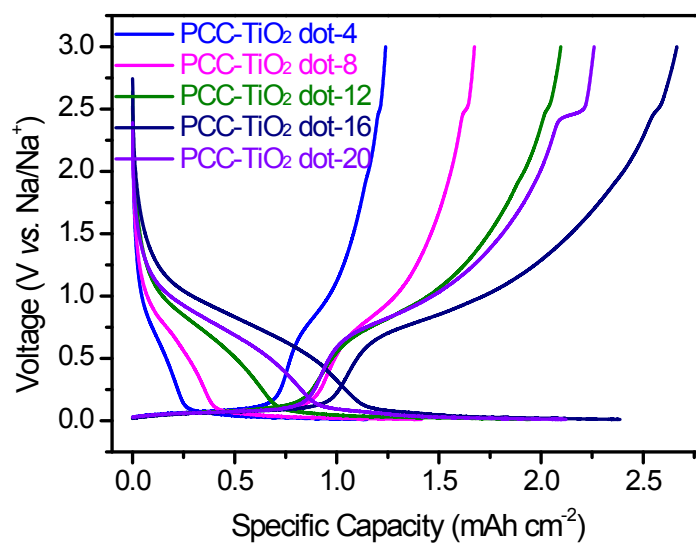


**Figure S7.** Charge-discharge curves of PCC-TiO<sub>2</sub> dot-4, PCC-TiO<sub>2</sub> dot-8, PCC-TiO<sub>2</sub> dot-12, PCC-TiO<sub>2</sub> dot-16, PCC-TiO<sub>2</sub> dot-20.

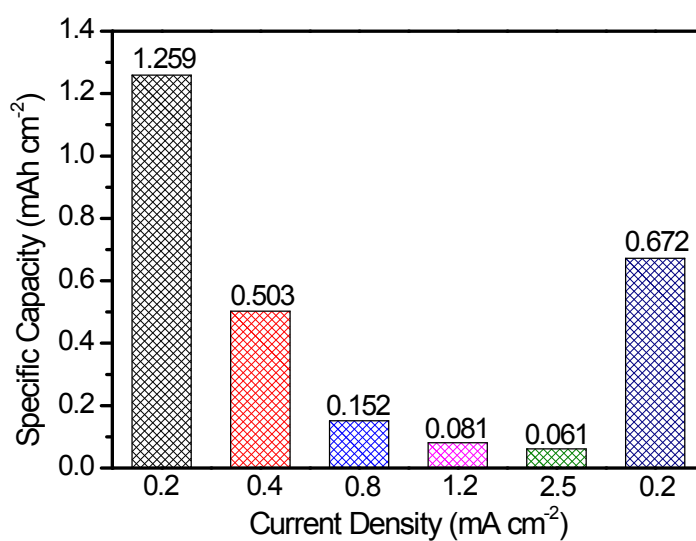


**Figure S8.** Discharge capacities of PCC in PCC-TiO<sub>2</sub> dot-16 at different current densities.

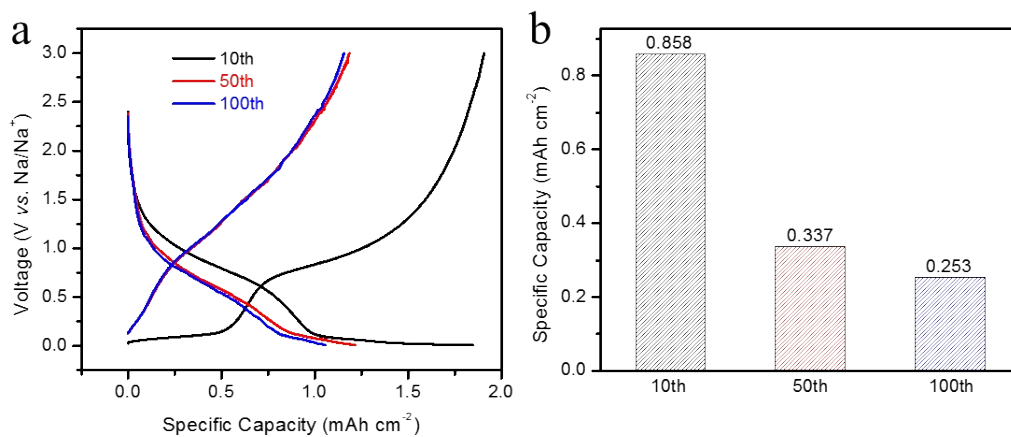


**Figure S9.** (a) Charge-discharge curves of PCC-TiO<sub>2</sub> dot-16 at current density of 0.2 mA cm<sup>-2</sup> and (b) discharge capacities of PCC in PCC-TiO<sub>2</sub> dot-16 at 10th, 50th, 100th cycles.

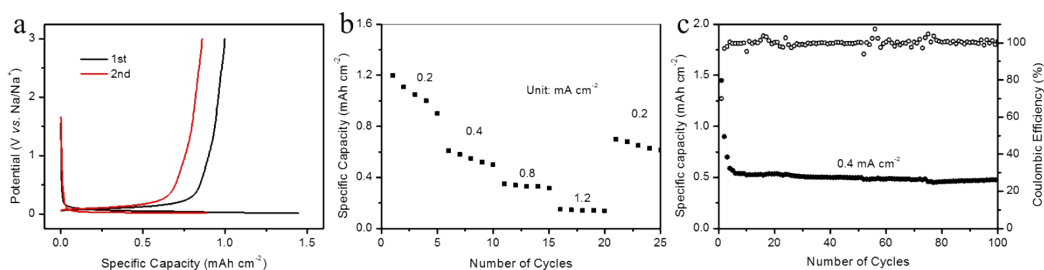


**Figure S10.** (a) Charge-discharge curves, (b) rate capability and (c) cycling performance of PCC.

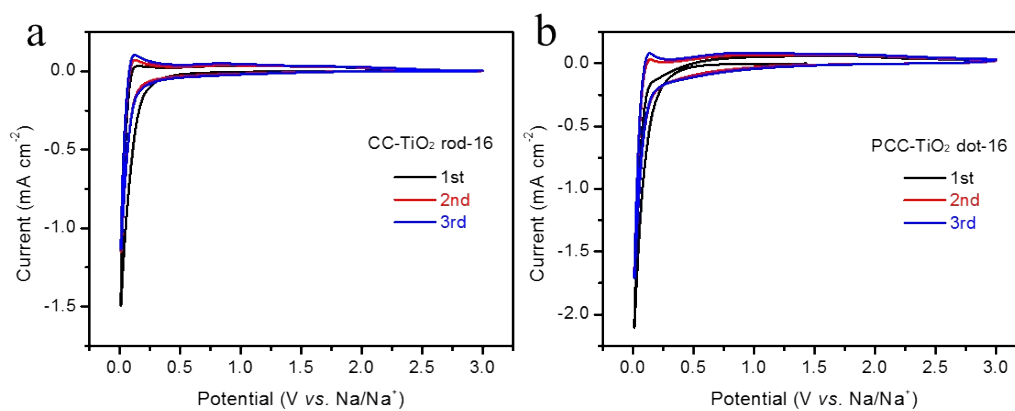


**Figure S11.** CV curves of (a) CC-TiO<sub>2</sub> rod-16 and (b) PCC-TiO<sub>2</sub> dot-16 with a scan rate of 0.1 mV s<sup>-1</sup>.

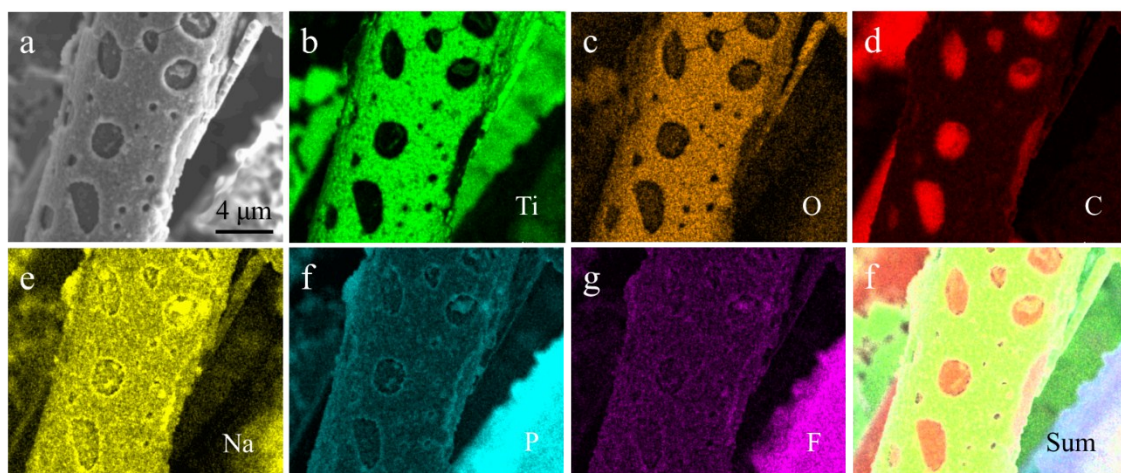


**Figure S12.** Elemental mappings of PCC-TiO<sub>2</sub> dot-16-after.

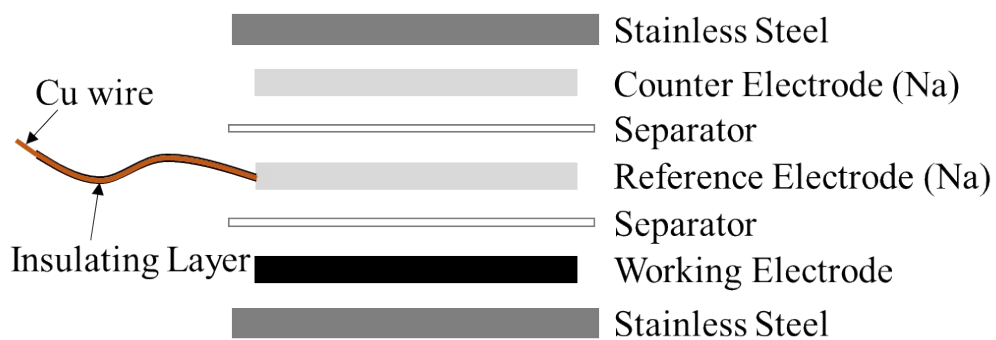


**Figure S13.** Schematic diagram of a three-electrode cell.



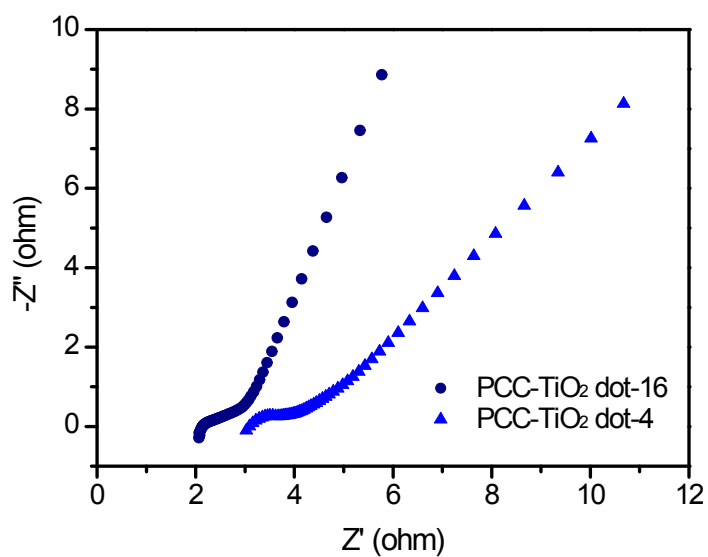


**Figure S14.** Nyquist spectra of PCC-TiO<sub>2</sub> dot-4 and PCC-TiO<sub>2</sub> dot-16 after 5cycles.

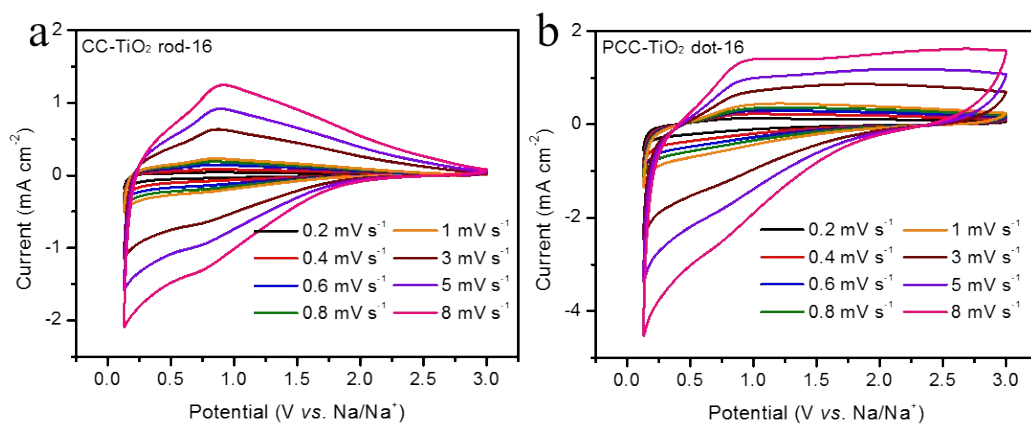


**Figure S15.** CV curves of CC-TiO<sub>2</sub> rod-16 and PCC-TiO<sub>2</sub> dot-16.

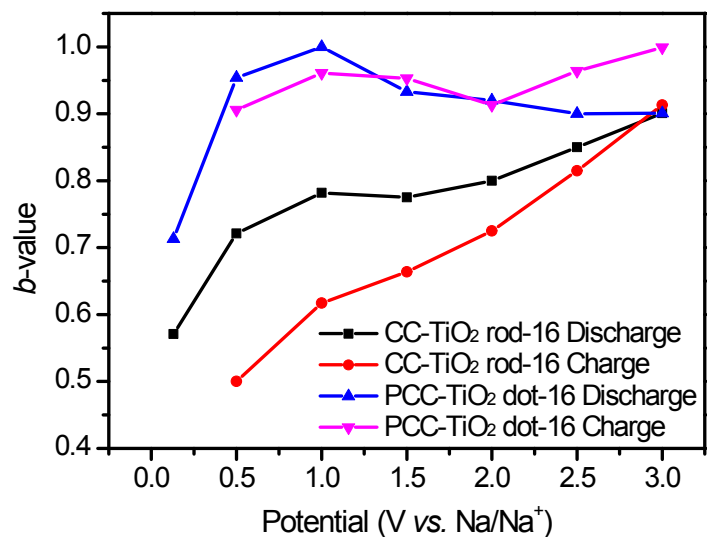


**Figure S16.** *b* values of the electrode at different SOC.

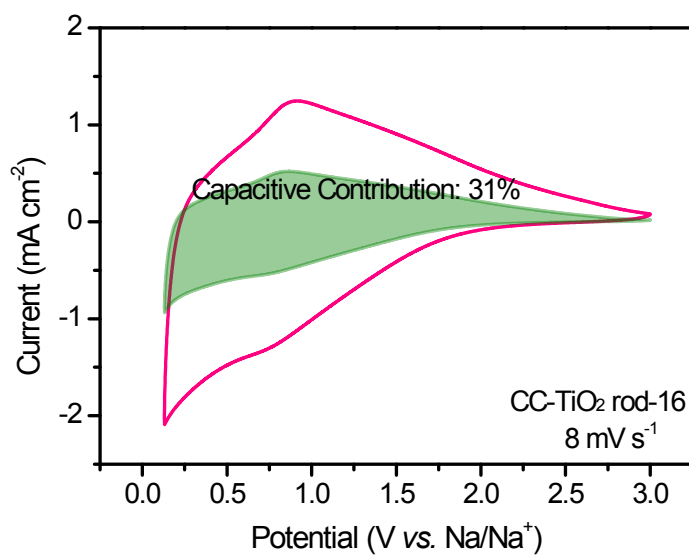


**Figure S17.** Quantitative analysis of capacitive contribution of CC-TiO<sub>2</sub> rod-16.

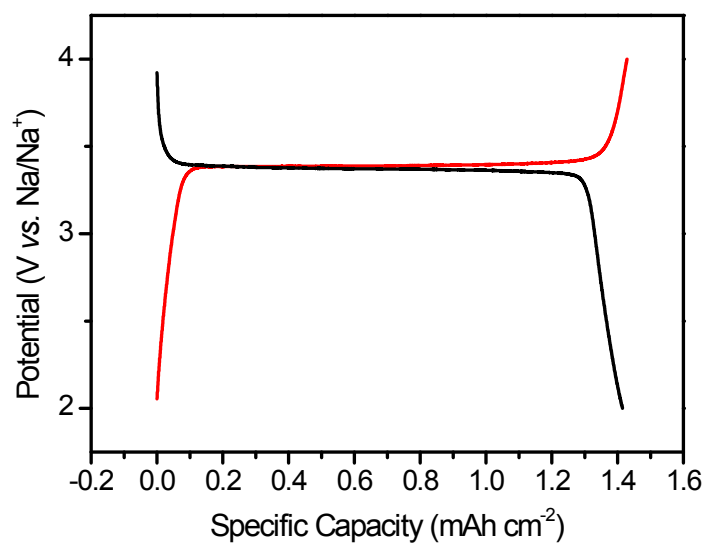


**Figure S18.** Charge-discharge curves of CC-NVPO.

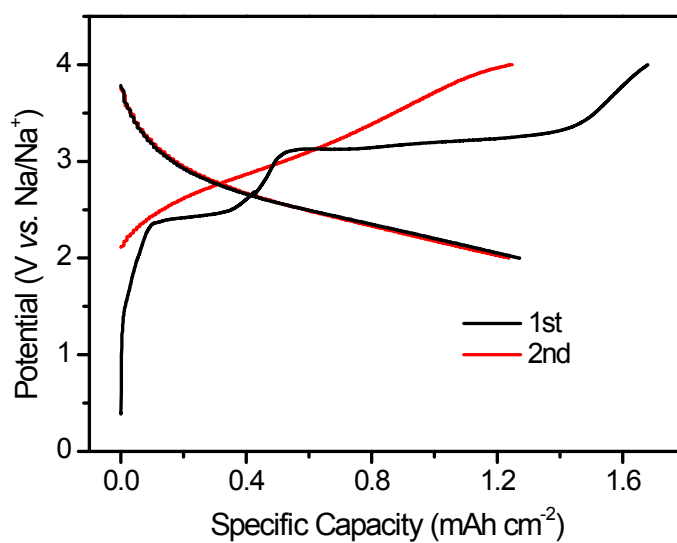


**Figure S19.** Charge-discharge curves of CC-NVPO || PCC-TiO<sub>2</sub> dot-16 full cell.

## References

1. H. S. Kim, J. B. Cook, H. Lin, J. S. Ko, S. H. Tolbert, V. Ozolins and B. Dunn, *Nat. Mater.*, 2017, **16**, 454.
2. B. Long, M. S. Balogun, L. Luo, W. Qiu, Y. Luo, S. Song and Y. Tong, *Adv. Energy Mater.*, 2018, **8**, 1701681.

3. D. Chao, C. Zhu, P. Yang, X. Xia, J. Liu, J. Wang, X. Fan, S. V. Saviolov, J. Lin, H. J. Fan and Z. X. Shen, *Nat. Commun.*, 2016, **7**, 12122.
4. J. Wang, S. Dong, B. Ding, Y. Wang, X. Hao, H. Dou, Y. Xia and X. Zhang, *Nat. Sci. Rev.*, 2017, **4**, 71.
5. F. Su, X. Li, W. Zhou, W. Chen, H. Li, Y. Cong, Z. Hong, Z. Qi and L. Li, *Polymer*, 2013, **54**, 3408.
6. S. Sangerlaub, K. Reichert, J. Sterr, N. Rodler, D. V. D. Haar, I. Schreib, C. Stramm, A. Gruner, J. Voigt and H. Raddatz, *Polym. Test.*, 2017, **65**, 142.
7. H. Shao, M. Zhang, W. Yao and B. Huang, *J. Polym. Res.*, 2012, **19**, 9919.
8. W. Chen, X. Li, F. Su, W. Zhou and L. Li, *J. Mater. Sci.*, 2013, **48**, 4925.